Hydration properties of $BaSn_{0.875}M_{0.125}O_{3-\delta}$ substituted by large dopants (M=In, Y, Gd, and Sm) from first principles

Émile Bévillon and Grégory Geneste
Laboratoire Structure, Propriétés et Modélisation des Solides, UMR CNRS 8580, Ecole Centrale Paris, Grande Voie des Vignes, 92295 Chatenay-Malabry Cedex, France

(Received 15 February 2008; revised manuscript received 11 April 2008; published 16 May 2008)

The hydration properties of barium stannate doped by trivalent elements (12.5%) are investigated by using density-functional calculations. The interaction energies of defects are computed in different relative positions, revealing that at this high doping level, similar to that currently used in experiments, the first-neighbor positions (between dopants and protons and between dopants and oxygen vacancies) are not always the most stable ones. The reasons for this unexpected energy landscape are analyzed in terms of structural distortions around dopants and dopant-proton and/or dopant-vacancy interaction overlaps. It is attributed to the large size of the dopants considered compared to that of Sn.

DOI: 10.1103/PhysRevB.77.184113 PACS number(s): 66.30.Dn, 71.15.Mb

I. INTRODUCTION

A better understanding of the microscopic mechanisms at the root of hydration processes in oxides is probably one of the key points that could help researchers to discover or design novel materials for proton conducting fuel cells. First-principles calculations in the framework of the density-functional theory are a powerful tool to approach the chemistry of hydration at the atomic scale in such materials. They are particularly suitable for the study of hydration and proton conduction in oxides since these phenomena involve point defects and are thus tractable within reasonable box sizes, as opposed to proton conducting hydrogen bonded networks, such as water, which would require very large supercell sizes. In the field of materials for fuel cells, first-principles calculations are mainly used in two manners: either *ab initio* molecular dynamics[1–5] or structural optimizations. In the last case, the structures studied are taken to their energy minimum with respect to the atomic displacements, giving access to some microscopic parameters. In particular, the entropic effects (vibrational or configurational) are not directly accessible to this kind of simulations. Up until now, these calculations have been extensively used to study the hydration properties and proton diffusion phenomena in various oxides[1–7] that have been used or tested as proton conducting materials (titanates, cerates, zirconates, niobates, etc.) with potential applications as electrolytes for fuel cells.

More than ten years ago, electronic structure calculations were applied by Münch *et al.*[2] to the study of proton dynamics in barium cerate,[1] barium titanate and barium zirconate, and then strontium titanate and calcium titanate,[3] through *ab initio* molecular dynamics in a tight-binding scheme. These authors pointed out the peculiar role of the O-O distance. Shimojo *et al.*[4,5] examined, also by using *ab initio* molecular dynamics, the diffusion of protons in Sc-doped $SrTiO_3$ and identified the differences in OH stretching vibration frequencies according to the location of the proton (near Ti or near the Sc dopant).

More recently, the chemical hydration process has been deeply investigated in barium zirconate: Björketun *et al.*[6,8] nicely studied the hydration of this compound doped by various trivalent elements (Gd, In, Nd, Sc, and Y) from first principles. In particular, they calculated the hydration energy in an independent defect model (-0.79 eV/H_2O) as well as the interaction energies between the dopants and both the oxygen vacancies and protons in the first-neighbor relative positions. They deduced hydration energies, within the framework of various models, and estimated the hydration Gibbs free energy by accounting for vibrational energetic and entropic effects. In a second work,[9] they studied the energy landscape of protons in the presence of various dopants in barium zirconate. They found a global attraction, which is stronger in the first-neighbor position except in the case of the biggest dopants considered (Y and Gd), for which the second-neighbor site is slightly more stable than the first-neighbor one.

Our aim is to apply the first-principles approach to another perovskite compound: $BaSnO_3$. The fundamental and practical interest for barium stannate $BaSnO_3$ has recently gained attention since interesting applications in water photolysis[10] and high pressure domain[11] have been suggested. The possibility of interesting hydration and proton conduction in this compound was experimentally demonstrated a few years ago.[12–14] In 50% In-doped [$BaIn_{0.5}Sn_{0.5}O_{2.75}$ (BISO)] and 50% Y-doped $BaSnO_3$ [$Ba_2YSnO_{5.5}$ (BYSO)], the hydration enthalpies have been measured to be -0.76 eV/H_2O (Ref. 13) and up to -1.05 eV/H_2O (Ref. 14) respectively, with also quite good proton conducting properties.

In this paper, we focus on the hydration properties of barium stannate doped with In, Y, Gd, and Sm. The results of Ref. 15 concerning La-doped $BaSnO_3$ are also taken into account for comparison and are completed. Our aim is (i) to investigate the hydration process in this compound for the different dopants by using density-functional calculations and study the energy landscape of protons and oxygen vacancies near the dopants, giving insight into original intrinsic structural effects and (ii) to study this hydration at large dopant concentration (here, 12.5%), giving access to the original effects that are possibly related to the proximity of the dopants inside the materials.

The simulation of isolated defects in oxides and semiconductors obeys rules and technicalities that are now well known and currently applied.[16–19] Their formation energies in the dilute limit are, in practice, usually calculated within periodic codes, and thus supercells are used, for which the dilute limit is obviously not reached. For instance, the isolated defects in perovskite oxides are often investigated with $2\times2\times2$ or $3\times3\times3$ supercells.[7] As a consequence, various corrections (Makov–Payne, potential alignment, etc.) may be applied to remove the artifacts that could be due to the small size of the supercells used.

Unfortunately, the materials used in fuel cells are very different since the properties that are searched (high ionic or protonic conductivity) require a *high concentration* of point defects. Typically, defects are present in host materials in quantities that can vary from a few percent to 50% (see Ref. 12 for examples of proton conductor oxides with substitution around 5%–10%). In such conditions, the dilute limit is obviously not reached, and the modelization of the system should take into account the interactions between the various defects present in the compound (H interstitials, O vacancies, and dopants).

In this work, we investigate dopants that are all bigger than the Sn atom they substitute. We evidence a nice effect for which we cannot clearly determine the cause yet: the most stable positions for oxygen vacancies and protons are in many cases found in the second-neighbor position rather than in the first-neighbor one. It seems to us that such a trend was suggested in the work of Björketun *et al.*[9] on $BaZrO_3$ in the case of Y and Gd dopants but was not so obvious as in barium stannate since Sn is smaller than Zr. After presenting the method and computational scheme in Sec. II, the results are presented and analyzed in Sec. III; in particular, the structural distortions, which could explain the effect mentioned in terms of hydrogen bond strength, are detailed. This is followed by a discussion in Sec. IV.

II. METHODOLOGY

A. Computational details

The calculations are performed in the framework of the density-functional theory[20] within the ABINIT code.[21] The electronic exchange and correlation effects are treated through the generalized gradient approximation (GGA) in the formalism of Perdew–Burke–Ernzerhof (PBE).[22] Troullier–Martins pseudopotentials[23] are used to account for the effects of core electrons. We treat $5s^2$, $5p^6$, and $6s^2$ for Ba, $5s^2$, and $5p^2$ for Sn, $4s^2$, $4p^6$, $5s^2$, and $4d^1$ for Y, $4d^{10}$, $5s^2$, and $5p^1$ for In, $5s^2$, $5p^6$, $6s^2$, and $4f^6$ for Sm, and $5s^2$, $5p^6$, $4f^7$, $5d^1$, and $6s^2$ for Gd as the valence electrons (semicore electrons are systematically taken into account for all of the dopants). All calculations are performed in a non-spin-polarized scheme by following the comments of Björketun *et al.*[9] We perform structural optimizations by using a plane-wave cutoff of 30 hartree (≈816 eV) and a k-point mesh corresponding to $4\times4\times4$ in the Brillouin zone of the five-atom perovskite cell. All our calculations are made by using a $2\times2\times2$ supercell containing about 40 atoms (according to the kind of defect considered: dopant, vacancy, or proton), in which we perform structural optimizations. The equilibrium lattice constant in the GGA-PBE approximation is found to be a_{eq}=4.156 Å for pure barium stannate [experiment: 4.116 Å (Ref. 24)], which is a typical overestimation within the GGA.

Our calculations are performed in cubic supercells with *fixed volume* ($2a_{eq}\times2a_{eq}\times2a_{eq}$). Thus, we model a 12.5% doped compound by a regular structure, in which the dopants are periodically distributed (one per supercell). This dopant content can be considered as a typical value in materials for fuel cells but with an obvious restriction imposed by the simulation technique: the system modeled in this way is a periodic distribution of dopants, whereas in most cases, the dopants are more randomly distributed in the host crystal (some exceptions may be found, for example, Y-doped barium stannate[14]). Anyway, we point out that clustering of dopants is rarely observed in these materials because such defects are charged in the acceptor-doped conditions: for instance, the possibility of having two dopants on neighboring sites has been investigated in Ref. 6 in barium zirconate. It was shown that large dopants are very rarely distributed on neighboring sites because of their large repulsion energy. This effect is all the more pronounced as the distribution reflects a low-temperature equilibrium. This strong repulsion supports the idea of a quite uniform distribution of substituting ions and can justify our periodic approach to simulate a high content of dopants in the materials. In $BaZrO_3$, this stands for dopant radii ≥0.80 Å, which is the case of the dopants in the present study (also, barium stannate has a smaller unit cell volume than barium zirconate).

B. Interaction between charged supercells

Part of the results presented hereafter concern charged defects (for instance, O vacancy, proton, or dopant). Such computations have been achieved according to the standard procedure by adding or removing the corresponding number of electrons from the supercell and, in order to avoid divergence of the electrostatic energy, by neutralizing the supercell with a uniform charged background (jellium). Such calculations may lead to quite a large error in the calculation of physical quantities, such as interaction or defect formation energies, because of long-range electrostatic interactions between charged defects periodically repeated.

An order of magnitude of the error caused by this artifact can be estimated by using the well known Makov–Payne correction.[25] For a defect with charge q, the first order term of this correction is proportional to q^2 and depends on the polarizability of the materials (the charged supercell effect is drastically lowered in a polarizable medium with respect to the vacuum),

$$E^{\mathrm{MP}} = E(L) + \frac{q^2\alpha}{2\epsilon_S L} + O(L^{-3}), \tag{1}$$

By using ϵ_S=22 for the static dielectric constant, as derived from the *ab initio* calculations for pure $BaSnO_3$,[11] the Makov–Payne correction for a defect with charge ±1 in the $2\times2\times2$ supercell is ≈0.11 eV. For a defect with charge +2 (for example, a charged oxygen vacancy), it reaches 0.44 eV.

This correction represents the interaction energy between a point charge periodically repeated and a jellium in a polarizable medium with dielectric constant ϵ_S. It may nevertheless drastically overestimate the interaction between periodically repeated charged defects[18] probably because the defect itself may be highly polarizable, much more than the undefective host materials. This correction is based on the hypothesis of point charge defects and does not account for the screening by the outermost electrons of the defect itself, for instance.[26] In most cases, the results obtained in the $2\times2\times2$ supercell are converged within a sufficient accuracy: for example, Sundell *et al.*[27] showed (in particular conditions) that the charged oxygen vacancy formation energy in barium zirconate does not vary from a $2\times2\times2$ to a $3\times3\times3$ supercell. Yet, the vacancy is twice charged and the supercell volume is multiplied by 3.375 in between. Thus, in what follows, both the corrected and uncorrected values of hydration energies are given.

C. Defect formation energies: hydration energy

The hydration energy of a compound can be defined starting from the formation energies of the different point defects created or destroyed along the chemical process. From a general point of view, the formation energy of a defect in a given host material depends on its charged state, on the external conditions (which fix the values of the chemical potentials of the atoms added or removed when the defect is formed), and, in the case of charged defects, on the Fermi level of the compound, since the removed or added electrons are taken or added at this energy level. The latter is a function of the general state of doping of the host crystal.

In this work, we first make several hypotheses to reproduce the experimental situation of hydration.

(i) The dopants M, which are trivalent elements, substitute Sn only (not Ba). This would mimic the synthesis of M-doped barium stannate under appropriate conditions for such a substitution (high μ_{Ba} and low μ_{Sn}).

(ii) We restrict the problem to acceptor-doped $BaSnO_3$, which implies that the Fermi level is close to the top valence band, and stabilizes the oxygen vacancies in a +2 charge state and the hydrogen interstitials in a +1 charge state (protons), as currently experimentally observed for this kind of materials.[28,29]

(iii) We also suppose that the process studied (hydration) is not simultaneous to other chemical reactions, such as oxidation by O_2 or reduction by H_2. This allows us to fix a relation between the O and H chemical potentials: $2\mu_H+\mu_O=E_{tot}(H_2O)$.

The formation energy of a given defect with charge q and involving addition or removal of atoms i is defined, in the dilute limit, by[16]

$$\Delta E_f(D^q) = E_{tot}(\text{host}+D;+q) - E_{tot}(\text{host};0) + \sum_i n_i\mu_i + q\mu_e,$$

where $E_{tot}(\text{host}+D;+q)$ is the energy of a $BaSnO_3$ supercell containing the defect D with charge q, $E_{tot}(\text{host};0)$ is that of a perfect uncharged supercell, μ_i is the chemical potential of the chemical species added or removed (according to the kind of defect), and μ_e is the chemical potential of the electrons (the Fermi energy). μ_e is usually referenced to the valence band maximum ϵ_{VBM} according to $\mu_e=\epsilon_{VBM}+\epsilon_F$. In defective supercells, due to periodic boundary conditions, the average Kohn–Sham potential is only defined up to a constant. For consistency with the undefective system, it is thus required to align the valence band maximum of the defective system to that of the undefective one.

If the supercell is large enough (dilute limit), one may use the valence band maximum of the perfect undefective and uncharged system ϵ^0_{VBM}, which is usually calculated as the energy difference between the perfect system and the charged (+1) undefective system. In fact, in the limit of large supercells, this difference tends to be the highest-occupied Kohn–Sham eigenvalue,[19] as a consequence of Janak's theorem.[30] However, in general, the supercell is not large enough to use ϵ^0_{VBM} without correction. Thus, an additional term must be used to correct $E_{tot}(\text{host}+D;+q)$ from the offset of the electronic band structure, which is usually estimated by $q\Delta V$, where ΔV is the difference of the mean potential between the defective and host systems at some well chosen point far from the defect.[18,19] Various methods can be used to estimate this correction; the most popular is a macroscopic average technique.[18] It can also be deduced from the shift in the eigenvalues of some well chosen eigenstates.[19]

In our case, the simulation of a high dopant content in $2\times2\times2$ supercells, as well as the simulation of pairs of defects in various sites of the supercell (especially dopant +oxygen vacancy), prevents us from a clear definition of a point "far from the defect" in the supercell. Thus, we prefer to use the method of Zywietz *et al.*,[31] which consists of aligning a low-energy *s*-like eigenstate (the semicore Ba 5*s* in our case). We emphasize that the application of this potential alignment correction leads to only a quite small modification of the final hydration energies given below (at most 0.2 eV). We stress that the main part of the following results, that is, the general form of the energy landscapes of O vacancies and protons, does not depend on the correction scheme used (any correction scheme leads to a constant shift of the whole energy landscape).

1. Hydration energy: independent defect model

To derive the formulas given hereafter, we assume that all of the corrections are included in the total energy expressions so that the electronic chemical potential is the same in all of the expressions. The formation energies of a hydrogen interstitial with a charge of +1 (proton), an oxygen vacancy with a charge of +2, and an M dopant (in substitution of Sn) with a charge of −1 can be written as

$$\Delta E_f(H^\bullet) = E_{tot}(\text{host}+H;+1) - E_{tot}(\text{host};0) - \mu_H + \mu_e, \tag{2}$$

$$\Delta E_f(V_O^{\bullet\bullet}) = E_{tot}(\text{host}+V_O;+2) - E_{tot}(\text{host};0) + \mu_O + 2\mu_e \tag{3}$$

$$\Delta E_f(M'_{\mathrm{Sn}}) = E_{\mathrm{tot}}(\mathrm{host} + M_{\mathrm{Sn}}; -1) - E_{\mathrm{tot}}(\mathrm{host}; 0) + \mu_{\mathrm{Sn}} - \mu_M - \mu_e. \quad (4)$$

In these equations, $E_{\mathrm{tot}}(\mathrm{host}+\mathrm{H};+1)$, $E_{\mathrm{tot}}(\mathrm{host}+V_{\mathrm{O}};+2)$, and $E_{\mathrm{tot}}(\mathrm{host}+M_{\mathrm{Sn}};-1)$ are the total energies of charged supercells, which contain, respectively, a single proton (charge of +1), a single oxygen vacancy (charge +2), and a single M dopant (substituting a Sn atom: charge of −1), $E_{\mathrm{tot}}(\mathrm{host};0)$ is the total energy of the supercell without defect (and uncharged), μ_i are the atomic chemical potentials, and μ_e is the Fermi energy.

The hydration energy, which corresponds to the well-known relation,

$$\mathrm{H_2O} + V_{\mathrm{O}}^{\bullet\bullet} + O_{\mathrm{O}}^{X} \rightarrow 2(\mathrm{OH})_{\mathrm{O}}^{\bullet}, \quad (5)$$

may be defined according to different schemes. First, we may consider that two protons are formed and an oxygen vacancy is suppressed independently of dopants. This leads to a simple model called no trapping model (NTM) in Ref. 6, in which the interaction between defects are neglected. In terms of defect formation energy, it can be written as

$$\Delta E_h^{\mathrm{NTM}} = 2\Delta E_f(\mathrm{H}^{\bullet}) - \Delta E_f(V_{\mathrm{O}}^{\bullet\bullet}). \quad (6)$$

By using Eqs. (2)–(4) and $2\mu_{\mathrm{H}}+\mu_{\mathrm{O}}=E_{\mathrm{tot}}(\mathrm{H_2O})$, it reduces to

$$\Delta E_h^{\mathrm{NTM}} = 2E_{\mathrm{tot}}(\mathrm{host} + \mathrm{H}; +1) - E_{\mathrm{tot}}(\mathrm{host}; 0) - E_{\mathrm{tot}}(\mathrm{host} + V_{\mathrm{O}}; +2) - E_{\mathrm{tot}}(\mathrm{H_2O}), \quad (7)$$

in which μ_e vanishes.

In this framework, the hydration energy $\Delta E_h^{\mathrm{NTM}}$ is obtained as the difference between twice the total energy of a supercell with one proton (charged +1) and the sum of total energies of a pure $BaSnO_3$ supercell, a supercell with a vacancy (charged of +2), and an isolated water molecule. The dopant is not accounted for in this model and the NTM hydration energy $\Delta E_h^{\mathrm{NTM}}$ roughly represents the intrinsic capability of the pure materials to catch water at its point defects (charged oxygen vacancies) independently of the dopant nature. In this simple model, we estimate the hydration energy of barium stannate to −0.69 eV/water molecule.

2. Interaction between defects

As already stated, the hydration of perovskites occurs through the presence of trivalent dopants, which are responsible for the existence of charge compensating oxygen vacancies (acceptor-doped conditions). Water molecules coming from the atmosphere dissociate into the vacancies, forming protonic charge carriers. In most cases, the dopants (charge of −1) attract both the oxygen vacancies (charge of +2) and the protons (charge of +1). Thus, in a more sophisticated model, which we call "total trapping model" (TTM), assuming that vacancies and protons are only trapped at dopant sites, the hydration energy should be better estimated by taking into account the interaction energies between (i) dopant and oxygen vacancy and (ii) dopant and protons. These interaction energies are classically defined[6] starting from the defect formation energies by

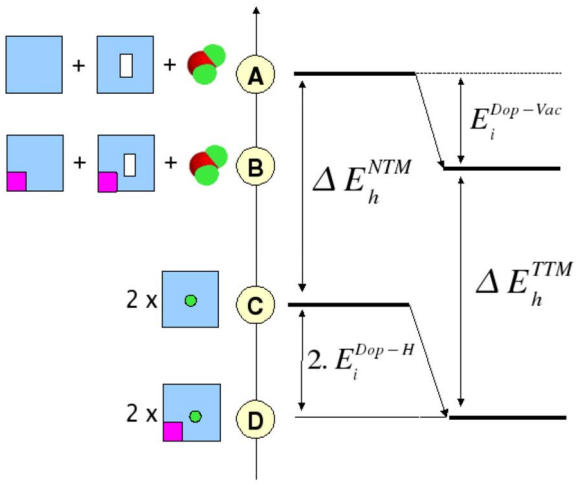

FIG. 1. (Color online) Schematic representation on an energy scale of the microscopic configurations used to estimate the hydration energies (only schematic since the energies of the systems drawn cannot be directly compared).

$$E_{\mathrm{int}}(M'_{\mathrm{Sn}}, \mathrm{H}^{\bullet}) = \Delta E_f(M'_{\mathrm{Sn}} + \mathrm{H}^{\bullet}) - \Delta E_f(M'_{\mathrm{Sn}}) - \Delta E_f(\mathrm{H}^{\bullet}), \quad (8)$$

$$E_{\mathrm{int}}(M'_{\mathrm{Sn}}, V_{\mathrm{O}}^{\bullet\bullet}) = \Delta E_f(M'_{\mathrm{Sn}} + V_{\mathrm{O}}^{\bullet\bullet}) - \Delta E_f(M'_{\mathrm{Sn}}) - \Delta E_f(V_{\mathrm{O}}^{\bullet\bullet}), \quad (9)$$

in which $\Delta E_f(M_{\mathrm{Sn}}^{-}+\mathrm{H}^{+})$ and $\Delta E_f(M_{\mathrm{Sn}}^{-}+V_{\mathrm{O}}^{\bullet\bullet})$ are the formation energies of the pairs of defects (M_{Sn}^{-},H^{+}) and $(M_{\mathrm{Sn}}^{-},V_{\mathrm{O}}^{\bullet\bullet})$, which are defined in the same way as that of the single defects.

By combining Eqs. (8) and (9) with Eqs. (2)–(4), the atomic chemical potentials vanish, and one gets

$$E_{\mathrm{int}}(M'_{\mathrm{Sn}}, \mathrm{H}^{\bullet}) = E_{\mathrm{tot}}(\mathrm{host} + M_{\mathrm{Sn}} + \mathrm{H}; 0) + E_{\mathrm{tot}}(\mathrm{host}; 0) - E_{\mathrm{tot}}(\mathrm{host} + M_{\mathrm{Sn}}; -1) - E_{\mathrm{tot}}(\mathrm{host} + \mathrm{H}; +1) \quad (10)$$

$$E_{\mathrm{int}}(M'_{\mathrm{Sn}}, V_{\mathrm{O}}^{\bullet\bullet}) = E_{\mathrm{tot}}(\mathrm{host} + M_{\mathrm{Sn}} + V_{\mathrm{O}}; +1) + E_{\mathrm{tot}}(\mathrm{host}; 0) - E_{\mathrm{tot}}(\mathrm{host} + M_{\mathrm{Sn}}; -1) - E_{\mathrm{tot}}(\mathrm{host} + V_{\mathrm{O}}; +2). \quad (11)$$

By using these definitions, the hydration energy may be modeled as

$$\Delta E_h^{\mathrm{TTM}} = \Delta E_h^{\mathrm{NTM}} + 2E_{\mathrm{int}}(M'_{\mathrm{Sn}}, \mathrm{H}^{\bullet}) - E_{\mathrm{int}}(M'_{\mathrm{Sn}}, V_{\mathrm{O}}^{\bullet\bullet}).$$

Accounting for such interactions, which are usually attractive, has two effects: First the dopant-vacancy interactions stabilize the nonhydrated system; the vacancies are considered as trapped at dopant sites. Second, the proton-dopant interactions stabilize the hydrated final system (Fig. 1).

By taking into account all of the previous definitions, the TTM hydration energy is finally written as

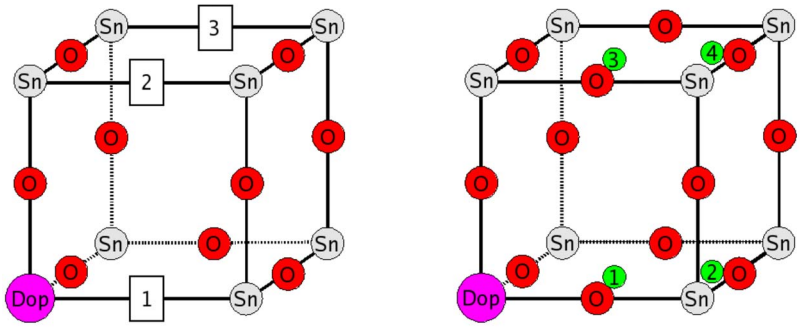

FIG. 2. (Color online) The different positions of proton and oxygen vacancy (with respect to the dopant) used to evaluate the interaction energies. For the protons, POS3 is obtained by a 90° rotation of POS2. The barium atoms have been removed from the figure for clarity.

$$\Delta E_h^{\mathrm{TTM}} = 2E_{\mathrm{tot}}(\mathrm{host} + M_{\mathrm{Sn}} + \mathrm{H};0) - E_{\mathrm{tot}}(\mathrm{host} + M_{\mathrm{Sn}} + V_{\mathrm{O}};$$
$$+ 1) - E_{\mathrm{tot}}(\mathrm{host} + M_{\mathrm{Sn}};-1) - E_{\mathrm{tot}}(\mathrm{H_2O}) \quad (12)$$

It can also be written as

$$\Delta E_h^{\mathrm{TTM}} = 2\Delta E_f(M'_{\mathrm{Sn}} + H^{\bullet}) - \Delta E_f(M'_{\mathrm{Sn}}) - \Delta E_f(M'_{\mathrm{Sn}} + V_{\mathrm{O}}^{\bullet\bullet}). \quad (13)$$

III. RESULTS

In order to compute the interaction energies between defects, one of the eight Sn atoms is replaced by a dopant (12.5% dopant content) in the supercell, leading to a uniform and periodic dopant distribution. Then, a defect (oxygen vacancy or hydrogen interstitial) is placed in the supercell, with different relative positions with respect to the dopant. Four configurations have been studied in the case of H^+ (denoted as POS1–POS4 by increasing proton-dopant distance); three in the case of $V_{\mathrm{O}}^{\bullet\bullet}$ (denoted as POS1–POS3 by increasing vacancy-dopant distance); they are shown in Fig. 2.

A. Dopant-oxygen vacancy interaction

The dopant-oxygen vacancy interaction energies are presented in Table I. The In and Y dopants present quite similar interaction energies, with a difference: the dopant-vacancy interaction energy is stronger in POS2 for Y and POS1 for In.

For the other dopants, the interaction energies are quite strong but their behaviors are singular. In the case of Sm and La, POS2 is the most stable configuration. The POS1 and POS3 configurations are energetically quite similar for Y and Sm but very different in the case of La. The case of Gd is specific too since the POS1 interaction energy is the strongest of all of the computed interaction energies, in spite of the absence of strong atomic rearrangement, and since the POS2 and POS3 energies are of the same order of magnitude.

TABLE I. Dopant-vacancy interaction energies (eV). The Shannon radii are taken from Ref. 32 and taken in the +3 oxidation state and the coordination number 6. For comparison, the Shannon radius of Sn^{4+} is 0.69 Å in the same coordinance. Bold: the most stable configuration.

Dopant	POS1	POS2	POS3	Shannon radius (Å)
In	−0.63	−0.56	−0.38	0.80
Y	−0.42	−0.75	−0.46	0.90
Gd	−1.81	−1.18	−1.19	0.94
Sm	−1.43	−1.54	−1.45	0.96
La	−1.13	−1.33	−0.57	1.03

B. Dopant-proton interaction

The problem of the location of stable sites for protons in perovskites is quite complex. In each site represented in Fig. 2, there might be in some oxides several stable sites, which differ from each other by the orientation angle of the OH group with respect to line joining two interoctahedral oxygens ([100]-type direction). In strontium titanate,[3–5] the stable position is reported as an OH group strongly bent with respect to this line. In cubic barium titanate and barium zirconate,[33] two stable sites are reported, the one bent, and the other exactly between two different octahedra. However, these positions have very close total energies (≤0.02 eV in GGA) and are separated by a very small barrier in the error bar of the calculation.[33] In the work of Björketun *et al.*[8] on barium zirconate, only one stable position is found in the (001) planes intersecting the octahedra, but other minima are found in the perpendicular planes containing Ba ions. Shi *et al.*[34] found three close stable positions for protons in In-doped barium zirconate near In dopants, all having exactly the same energy. In In-doped $CaZrO_3$ and $SrZrO_3$, these authors found one stable position. The potential energy surface of protons might therefore be quite complex and exhibit several stable sites around the line between two octahedra (one along this line and two symmetrically equivalent right and left), but these sites have very close energies, so that this apparent complexity can be ignored, at least in large perovskites (i.e., barium perovskites). In pure barium stannate, we have considered the position exactly between two octahedra and checked that it is stable. In doped barium stannate, especially in POS1 and POS2, the presence of the dopant breaks the symmetry and the OH group appears as bent with respect to this line.

The dopant-proton interaction energies are presented in Table II. They are all attractive. Except in the case of In, the POS2 position is the most stable for all of the dopants (Y, Gd, Sm, and La), and the interaction energies are still strong for POS3 or POS4. The magnitude of the interaction energy (in POS2) roughly increases with dopant radius.

TABLE II. Dopant-proton interaction energies (eV). Dopants are still ranged according to their Shannon radii. Bold: the most stable configuration.

Dop | Config.	POS1	POS2	POS3	POS4
In	−0.33	−0.31	−0.22	−0.22
Y	−0.21	−0.38	−0.26	−0.19
Gd	−0.36	−0.57	−0.33	−0.31
Sm	−0.46	−0.50	−0.40	−0.37
La	−0.33	−0.83	−0.46	−0.28

C. Hydration energies

Hydration energies are commonly computed by using the first-neighbor relative position (POS1) for the oxygen vacancy and for the proton since it is usually assumed that these configurations lead to the strongest interaction energies. In our case and at least for this special dopant distribution and concentration, we do not find these positions to be the most stable ones in most cases. Consequently, in order to be consistent, two hydration energies are calculated: (i) according to the standard way, using the first-neighbor position (POS1) for oxygen vacancy and proton, (ii) using the strongest dopant-vacancy and dopant-proton interaction energies, or, in other words, considering the most stable initial and final state for the hydration process. The results are gathered in Table III. The interaction energies in the case of In and Y imply corrections of the initial and final state that almost compensate each other (Fig. 2) so that finally the hydration energy (≈−0.70 eV) is close to that of the no trapping model (−0.69 eV).

The rare earth elements (Sm and Gd) exhibit weak values of hydration energy, which are positive in some cases. This is mainly due to the strong dopant-oxygen vacancy interaction (≈−1.5 eV); the lacunar initial state is very stable compared to the hydrated final state. The case of La is particular because a weak hydration energy is found in case (1) where only the first-neighbor interaction energies are accounted for (−0.22 eV), whereas in case (2), the hydration energy is lowered to −1.02 eV especially because the proton strongly interacts with La in the second-neighbor position (interaction energy of −0.83 eV).

TABLE III. Hydration energies of acceptor-doped $BaSnO_3$ (eV/H_2O). (1) is an estimation of the hydration energy using the first-neighbor configuration, and (2) indicates that the strongest defect interactions have been considered. ∞ refers to the no trapping model (pure $BaSnO_3$), and thus does not depend on the dopant. In brackets: the Makov–Payne correction is added. The experimental hydration enthalpies are added for comparison when available, with the corresponding content of dopants.

Dopant	(1)	(2)	∞	expt ΔH^0
In	−0.71 (−0.93)	−0.71 (−0.93)	−0.69	−0.76[13] (50%)
Y	−0.69 (−0.91)	−0.70 (−0.92)	−0.69	−1.05[14] (50%)
				−0.62[12] (10%)
Gd	+0.40(+0.18)	−0.02(−0.24)	−0.69	
Sm	−0.16(−0.38)	−0.14(−0.36)	−0.69	
La	−0.22(−0.44)	−1.02(−1.24)	−0.69	

At this stage, comparisons to the experimental values can be made, keeping in mind that the hydration energy is known to be dopant concentration dependent.[12] To our knowledge, experimental data for precisely 12.5% dopant content in substituted barium stannate do not exist, but some results can be found for different dopant concentrations, such as BISO, which corresponds to a 50% In-doped $BaSnO_3$ or BYSO for a [10%;50%] Y-doped $BaSnO_3$.

In the case of Y, changes are observed when the concentration of dopants is varied. The hydration energy of BYSO at 10% is ≈−0.62 eV and reaches −0.83 eV at 25%.[12] For 50%, it is measured to be ≈−1.05 eV. The agreement with the present computations is thus quite good. In the case of In, we only have the experimental value for the 50% dopant concentration (ΔH=−0.76 eV from Ref. 13); thus, it is difficult to compare our theoretical value to the experimental one. However, having similar interaction and hydration energies, we suggest that similar trends for In and for Y are expected.

D. Structural distortions

A finer understanding of the interactions presented above can be obtained from the analysis of the structural distortions around the defects. The nature of the attractive interaction between protons and trivalent dopants has been attributed to electrostatics for a long time, since both defects are charged with opposite sign[35] in acceptor-doped conditions. However, this is not so clear because the difference between nominal charges and real charges (that can be obtained, for example, from the integration of the electronic density) is large in ionocovalent solids. Other phenomena can contribute to the interaction between charged defects. In particular, the interaction energy may include an elastic contribution, which is caused by the local distortions induced by the presence of the defects. These elastic interactions can be investigated from the local distortions induced by the dopants. As a function of the dopant, these geometric modifications may vary a lot.

1. Dopant-oxygen vacancy pair

The local distortions in the case of dopant-oxygen vacancy interaction are gathered in Table IV. In particular, we are interested in the distance between the cations surrounding the vacancy (one of these cations is the dopant in the case of POS1, and they are Sn atoms in all other cases). The angles α and β correspond to the average of the four $O\text{-}Elt_1\text{-}Elt_2$ angles and the four $O\text{-}Elt_2\text{-}Elt_1$ angles, respectively (see Fig. 3).

The distance between the cations surrounding the vacancy (in POS1) is an indicator of how "charged" the dopant is with respect to Sn in barium stannate. In this position, the distance is reduced with respect to the $BaSnO_3$ GGA cell parameter (4.156 Å) in the case of Gd, Sm, and La. The case of In and Y is different since the distance between the dopant and the Sn beside the vacancy is now higher than 4.156 Å, and the α and β angles are close to their value in the absence of dopant (82.1°).

TABLE IV. Structural distortions in the case of a dopant and an oxygen vacancy in the supercell. The angles α and β refer to Fig. 3. $Elt_1 \diamond Elt_2$ is the distance between the cations Elt_1 and Elt_2.

Dopant	In	Y	Gd	Sm	La
		POS1			
$Elt_1 \diamond Elt_2$(Å)	4.34	4.32	4.00	3.91	4.09
α(°)	84.9	86.0	93.4	91.0	95.2
β(°)	81.4	81.1	84.0	92.8	79.1
		POS2			
$Elt_1 \diamond Elt_2$(Å)	4.40	4.40	4.31	4.18	4.38
α(°)	81.3	81.5	84.6	95.2	79.8
β(°)	82.0	81.8	85.0	82.5	82.1
		POS3			
$Elt_1 \diamond Elt_2$(Å)	4.41	4.40	4.30	4.14	4.39
α(°)	81.8	81.8	84.7	85.8	81.6
β(°)	81.9	81.9	85.7	91.9	81.8
		Infinity (NTM)			
$Elt_1 \diamond Elt_2$(Å)	4.41				
α(°)	82.1				
β(°)	82.1				

The distance between these cations might be interpreted in terms of an electrostatic interaction: it probably increases with the net charge of the dopant since the vacancy does not contain electrons ($V_O^{\bullet\bullet}$ defect). Thus, we may suppose that Gd, Sm, and La are less charged (formally closer than +3) than In and Y. We note that all these distances are lower than the Sn-Sn distance surrounding a vacancy (4.41 Å), which is in agreement with the fact that the trivalent dopants are less charged than Sn.

By considering the other configurations (POS2 and POS3), weaker distances and weak angle variations for In, Y, Gd, and La are observed. In particular, the distance between the cations surrounding the vacancy recovers a value very close to 4.41 Å for In and Y in POS2 and further positions. In the same manner, the α and β angles are close to 82° in these positions. Also, we observe an interesting behavior of the Sm-doped structures since the distortions remain strong even in POS2: Sn ◇ Sn distances are still short and the angle variations are still strong, indicating that the tin atoms may be partially reduced. The same phenomenon occurs in the POS3 configurations.

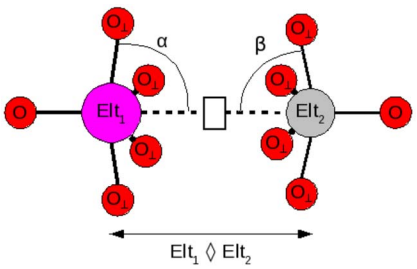

FIG. 3. (Color online) Definition of the α and β angles used in Table IV. These angles are the averages of the four-$O_\perp$-Elt_i-◇ angles. Elt_1 is the Sn closest to the dopant, and in the case of POS1, Elt_1 is the dopant.

2. Dopant-hydrogen interstitial pair

Local distortions around the proton are of primary interest since they can enlighten why interactions in the case of the POS2 configuration are stronger than in POS1. They are described in Table II. Figure 4 illustrates the geometry and local distortions around the dopant in the presence of a hydrogen interstitial with a charge of +1.

We first compare local distortions around the proton in the POS1 and POS2 configurations, which is particularly relevant since the proton, its oxygen, and the dopant are in the

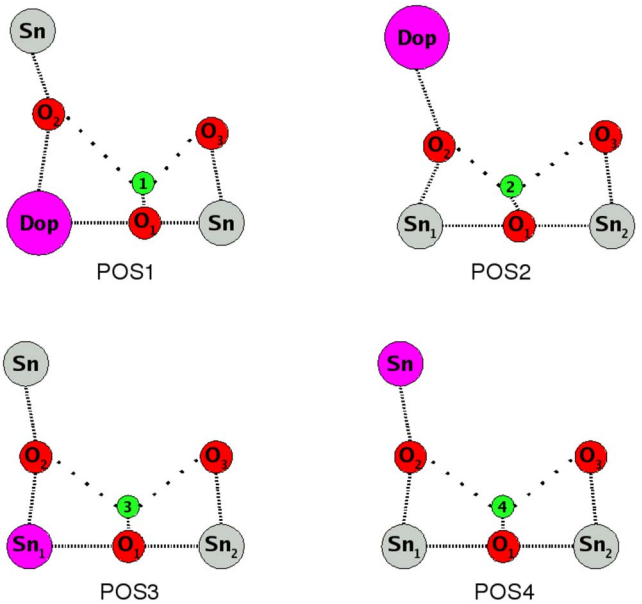

FIG. 4. (Color online) Local environment of the proton in the different configurations. The purple tin atoms indicate that a dopant is upper and under the tin.

TABLE V. Structural distortions in the case of a dopant and a hydrogen interstitial in the supercell.

Dopant	In	Y	Gd	Sm	La
		POS1			
H-O_2(Å)	2.06	2.22	2.14	2.18	2.21
H-O_3(Å)	2.15	2.03	2.02	1.86	1.90
Dop-O_2(Å)	2.20	2.21	2.21	2.18	2.32
O_2-Dop-O_1(°)	78.3	80.8	78.6	77.2	77.1
O_3-Sn-O_1(°)	80.8	79.9	79.1	75.8	77.5
Dop-O_1-H(°)	82.7	85.9	83.1	97.1	93.7
		Average			
H-O(Å)	2.11	2.12	2.08	2.02	2.06
		POS2			
H-O_2(Å)	1.94	1.96	1.72	1.85	1.74
H-O_3(Å)	2.16	2.14	2.27	2.17	2.22
Dop-O_2(Å)	2.21	2.24	2.35	2.23	2.35
O_2-Sn_1-O_1(°)	77.6	78.4	72.5	75.3	73.2
$O_3-Sn_2-O_1$(°)	81.1	81.2	83.5	81.2	83.1
Sn_1-O_1(°)	82.3	81.6	72.5	80.6	72.5
		Averages			
H-O(Å)	2.05	2.05	1.99	2.01	1.98
		POS3			
Sn_1-O_1-H(°)	87.7	85.7	88.6	89.3	81.8
		Averages			
Sn-O(Å)	2.11	2.11	2.09	2.09	2.13
H-O(Å)	2.11	2.12	2.11	2.11	2.15
O-Sn-O(°)	80.0	80.4	80.7	80.5	80.9
		POS4			
Sn_1-O_1-H(°)	87.8	86.5	89.9	89.3	80.8
		Averages			
Sn-O(Å)	2.08	2.07	2.10	2.09	2.06
H-O(Å)	2.09	2.09	2.12	2.11	2.08
O-Sn-O(°)	79.9	80.5	80.6	80.2	79.9
		Infinity (NTM)			
H-O_2(Å)	2.11				
O-Sn-O(°)	80.2				
Sn-O_1-H(°)	89.6				

same [001] plane. We will see that the reinforcement of hydrogen bonds with the oxygens in this plane will or will not be allowed according to the size of the dopant.

The dopants, in their +III formal oxidation state, are bigger than tin in its +IV formal oxidation state in the sixfold coordination, in agreement with the corresponding Shannon radii (given in Table I). This means that they are likely to push their first-neighbor O atoms away, as it can be seen from the Dop-O_2 distance (Table V) that all are $\geq$2.08 Å (the Sn-O distance in pure $BaSnO_3$ in GGA).

Due to the size of the dopant, the H-O_2 distances increase in POS1 (with respect to the situation where no dopant is present). Except for the case of In (too small) the H-O_3 distance tends to decrease (1.86–2.03 Å) and is smaller than H-O_2 in POS1. Exactly the opposite phenomenon occurs in POS2, in which H-O_2 is smaller than H-O_3. The distances are detailed in Table V. Let us take the example of the Y dopant: in POS1, H-O_2 (resp. H-O_3)=2.22 Å (resp.2.03 Å), whereas in POS2, H-O_2 (resp. H-O_3)=1.96 Å (resp. 2.14 Å). The average H-bond length is significantly shorter in POS2 than in POS1. This original effect due to the large size of the dopants is schematically described in Fig. 4. It is present for all dopants studied except for In (almost the same size as Sn).

This effect is also related to strong angle variations: in POS2, the O_2-Sn_1-O_1 angle is decreased compared to the O_2-Dop-O_1 angle in POS1; the Sn_1-O_1-H angle (in POS2) is also decreased with respect to the Dop-O_1-H angle (in POS1). The O_3-Sn_2-O_1 also increases. These variations tend to almost align the O_2, H, and O_1 atoms in POS2 and considerably reduce the O_2-H distance to short hydrogen bonds, of the same order of magnitude as in water (1.76 Å), espe-

cially in the case of Gd and La (1.72 and 1.74 Å respectively). The exact opposite phenomenon occurs in the case of POS1, in which, as a consequence, the O_3, H, and O_1 tend to align, which decreases the H-O_3 distance. However, this effect is not so amplified as in the POS2 case.

Thus, the average of the hydrogen bond lengths decreases from POS1 to POS2, reflecting stronger interactions of this kind in POS2. In spite of the general trend found for these angles and distances, the structural distortion implies that the phenomenon is dopant size-dependent. Large dopants (such as La) create stronger distortions and amplify the phenomenon, leading to stronger interaction energies in POS2, whereas small dopants (such as In) create weak distortions and the interaction energies in POS2 do not change significantly with respect to POS1.

Concerning POS3 and POS4, the distortions are quite similar. The O_1-H, the Sn-O, and the H-O average distances and the O-Sn-O average angles are very close to those of the hydrated $BaSnO_3$ in the NTM model. The main local distortion is for the Sn_1-O_1-H angle, which varies from 80.8 to 92.4° depending on the dopant, but no correlation can be found with the variation of the interaction energy.

IV. DISCUSSION

A. Most stable sites of protons near dopants: first or second neighbor?

In the case of Y, La, Sm, and Gd, we have seen that the most stable positions for the protons have been found in the second-neighbor position (POS2) rather than in the first neighbor one (POS1). This is quite unexpected since the interaction between dopants with charge −1 and protons with charge +1 is supposed to be mainly of electrostatic nature and thus less attractive when the distance increases. The same arguments may apply to the interaction between oxygen vacancies (charge +2) and dopants.

The strength of the hydrogen bonds, on average shorter in the second-neighbor position, seems to play a role in the related stronger interaction. The presence of large dopants (with respect to Sn) seems to be responsible for the distortions that lead to this peculiar energy landscape. The effect is particularly important here probably because the dopants we test are significantly larger than Sn. We note that a similar effect, but much smaller, was recently reported by Björketun *et al.*[9] in the case of $BaZrO_3$ doped by Y and Gd. The effect is smaller probably because the difference in size between Y/Gd (Shannon ionic radii 0.90 and 0.94 Å) and Zr^{4+} is smaller than that with Sn, which can also be seen from the lattice constant (4.25 Å for $BaZrO_3$, 4.156 Å for $BaSnO_3$ in GGA).

Anyway, in the supercell we use $(2\times2\times2)$, the proton in the second-neighbor position (POS2) is almost at mid-distance between two dopants which are periodic image from each other. Thus, in the strong interaction found in POS2, there could also be a contribution from the overlap between the interactions with the *two* dopants. The small size of the supercell we use unfortunately prevents us from making a conclusion.

However, the computed energy landscape is relevant for the 12.5% doping content simulated here, provided the distribution of dopants is quite uniform (we note that an ordering of the dopants has been observed in the case of Y-doped barium stannate[14]). It suggests that the low-energy pathways for the diffusion of protons contain the second-neighbor relative positions. For large dopants, the shorter H-O_2 distances compared to those of H-O_3 in POS2 suggest a lower activation energy for the hydrogen jump from O_1 to O_2 than from O_1 to O_3. In other words, this means that after structural rearrangement, the hydrogen in POS2 might migrate more easily from POS2 to POS1 than from POS2 to POS2. Observation of hydrogen bonds in POS1 suggest, as opposed to POS2, that after structural rearrangement, the migration of the hydrogen from POS1 to POS2 would be favored compared to the POS1-POS1 jump (H-$O_3 \leq$ H-O_2).

If such displacements are accompanied by rotational diffusion (i.e., if the activation energies for rotation are less high than those for jumps), large dopants would have to be considered not as trapping sites for hydrogen but as dynamic points inside of the materials, facilitating the displacements of protons. As a consequence, the percolation of protons throughout the crystal would be easier to achieve, and a high dopant-proton interaction energy may not necessarily mean strong trapping (and thus high activation energy for conduction) since protons at the vicinity of dopants could escape more easily. On the other hand, if strong activation energy for rotational diffusion is found, which is likely since the strong hydrogen bonds observed could have for additional effect to constrain hydrogen displacements in the O_2-O_1-O_3 plane (Fig. 4), the favored POS1 to POS2 and POS2 to POS1 displacements of protons should be viewed as a back-and-forth movement leading to the trapping of the protons in the vicinity of dopants (POS1 and POS2).

Interestingly, the present results could be a motivation to perform x-ray absorption spectroscopy experiments on hydrated barium stannate and get information on the location of protons and vacancies in this compound doped with large dopants. Such methods have been recently employed on Y-doped $BaCeO_3$ (Refs. 36 and 37) and showed a preferential location of the protons near dopants, confirming the expected attractive interaction between acceptor dopants and protons. Barium cerate is nevertheless a strongly distorted structure (orthorhombic), and the ionic radius of Y^{3+} (0.90 Å) is close to that of Ce^{4+} (0.87 Å) in octahedral coordinance. Thus, Y (and also Gd) in $BaCeO_3$ cannot be considered as a large dopant and the trends of the present article probably do not apply to this peculiar compound. In the neighborhood of the defects (dopant, vacancy, and hydrogen), the bond lengths are strongly increased or decreased, especially in the case of the hydrogen interstitial, due to the strong interactions with neighboring oxygens, and more generally, in the case of close interacting defects. As a consequence, this makes the system more and more inhomogeneous, in particular, for the oxygen bond lengths, as clearly evidenced by Giannici *et al.*[37] in an experimental way.

B. Hydration enthalpy as a function of the dopant

The contribution of the dopant-proton and dopant-vacancy interaction energies to the hydration energy is im-

portant and may even lead to strong deviations from the NTM value, except for indium and yttrium where the effect of H-dopant and vacancy-dopant counterbalance each other. The hydration energy calculated for Y is close to the experiment and in qualitative agreement with the case of In.[13,14]

The case of rare-earth elements is interesting: these dopants are characterized by very strong interaction energies with oxygen vacancies. By contrast, the interaction energies with protons are not so high. This contributes to a strong stabilization of the nonhydrated structure in the TTM model and thus considerably diminishes the hydration energy with respect to the NTM value.

The hydration energy, which is close to the standard hydration enthalpy,[15] is unfortunately not sufficient to determine the proton content as a function of temperature and water partial pressure under equilibrium conditions. However, the level of hydration, that is, the quantity of water molecules dissolved in the materials at a given water pressure and temperature, also depends on the standard entropy ΔS^0 of the chemical reaction. The latter is, unfortunately, not accessible from the present calculations and should be modeled. The characteristic values of ΔS^0 are in the range of ≈ -70 to -180 J mol^{-1} K^{-1} in hydrated perovskites. This quantity drastically influences the hydration properties.

V. CONCLUSION

In this work, we have investigated the hydration mechanisms of $BaSnO_3$ doped with various trivalent elements within density-functional calculations. An unexpected energy landscape for the protons is found, in which the dopant-proton second-neighbor position is the most stable for many dopants. Similarly, in many cases, the dopant-vacancy interaction energy is higher in the second-neighbor position. At this stage, it seems that both the peculiar distortions due to the substitution by large dopants and the interaction overlaps (due to the high concentration of dopants) are acting in the phenomenon. Calculations are currently in progress on larger supercells to discriminate between the two processes and determine the weight of each one.

In particular, we have shown that the hydrogen bonds are on average shorter and thus stronger in the second-neighbor relative positions. However, we do not think that these distortions are the only contribution. Indeed, the enhancement of two hydrogen bonds can probably not explain certain cases such as La doping, in which the H-La interaction energy is more than twice enhanced in the second-neighbor compared to the first-neighbor position. Thus, the interaction overlap is also probably important.

This interaction overlap is also suggested by the experimental increase in ΔH^0 with respect to the dopant content. This is, in particular, related by Kreuer[12] in the case of $BaSnO_3$ and $BaCeO_3$ doped by yttrium. For example, ΔH^0 varies from ≈ -60 to ≈ -90 kJ/mol in $1/2(Ba_2Sn_{2-x}Y_xO_{5.5})$ between $x \approx 0.05$ and $x=0.2$, while for barium cerate ($BaCe_{1-x}Y_xO_{3-\delta}$), which intrinsically hydrates much more than stannates and zirconates, the hydration enthalpy varies from ≈ -130 to ≈ -180 kJ/mol between low doping and $x=0.2$. This variation of the hydration enthalpy is usually interpreted in terms of *basicity* of the oxide, which increases with doping content. It has been confirmed by phenomenological calculations in the case of barium cerate[38] and calcium and/or strontium zirconate.[39]

However, in the case of large dopants, the stabilization of second-neighbor positions for protons (and oxygen vacancies in most cases), and the strong interaction energies for all of the other configurations seem to us an important result. It suggests that the diffusion pathways for protons do not necessarily contain a single position, which is close to the dopant, in which the interaction would be so strong that it traps the hydrogen.[35] Instead, one has to consider that this diffusion pathway is highly modified, even at quite a large distance, by the simultaneous presence of hydrogen and dopant and by the size of the dopant.

More calculations are required to make precise the microscopic mechanisms at the origin of the hydration processes in oxides and especially to understand the role played by interaction overlaps and by the interaction between single dopants and protons. In particular, the computation of activation barriers for proton jump and diffusion are necessary to have an understanding of proton conduction in doped barium stannate. This will help us to understand the dopant content evolution of the hydration properties in such materials in detail and could guide researchers in their choice of appropriate dopants.

ACKNOWLEDGMENTS

The authors thankfully acknowledge the computer resources, technical expertise, and assistance provided by the Barcelona Supercomputing Center—Centro Nacional de Supercomputación. Part of the calculations has been performed, thanks to the facilities of the CNRS Supercomputing Center (IDRIS) under Project No. 082030.

[1] W. Münch, G. Seifert, K. D. Kreuer, and J. Maier, Solid State Ionics **86-88**, 647 (1996).
[2] W. Münch, G. Seifert, K. D. Kreuer, and J. Maier, Solid State Ionics **97**, 39 (1997).
[3] W. Münch, K. D. Kreuer, G. Seifertli, and J. Majer, Solid State Ionics **125**, 39 (1999).
[4] F. Shimojo, K. Hoshino, and H. Okazaki, Solid State Ionics **113-115**, 319 (1998).
[5] F. Shimojo and K. Hoshino, Solid State Ionics **145**, 421 (2001).
[6] M. E. Björketun, P. G. Sundell, and G. Wahnström, Faraday Discuss. **134**, 247 (2007).
[7] See, for instance (Ref. 6) and C. Shi, M. Yoshino, and M.

Morinaga, Solid State Ionics **176**, 1091 (2005) for zirconates and P. Erhart and K. Albe, J. Appl. Phys. **102**, 084111 (2007) for barium titanate.
[8] M. E. Björketun, P. G. Sundell, G. Wahnström, and D. Engberg, Solid State Ionics **176**, 3035 (2005).
[9] M. E. Björketun, P. G. Sundell, and G. Wahnström, Phys. Rev. B **76**, 054307 (2007).
[10] P. H. Borse, J. S. Lee, and H. G. Kim, J. Appl. Phys. **100**, 124915 (2006).
[11] E. Bevillon and G. Geneste, Phys. Rev. B **75**, 214106 (2007).
[12] K. D. Kreuer, Solid State Ionics **125**, 285 (1999).
[13] T. Schober, Solid State Ionics **109**, 1 (1998).
[14] P. Murugaraj, K. D. Kreuer, T. He, T. Schober, and J. Maier, Solid State Ionics **98**, 1 (1997).
[15] E. Bévillon, G. Geneste, A. Chesnaud, Y. Wang, and G. Dezanneau, Ionics (to be published).
[16] S. B. Zhang and J. E. Northrup, Phys. Rev. Lett. **67**, 2339 (1991).
[17] A. García and J. E. Northrup, Phys. Rev. Lett. **74**, 1131 (1995).
[18] C. G. Van de Walle and J. Neugebauer, J. Appl. Phys. **95**, 3851 (2004).
[19] C. Persson, Y.-J. Zhao, S. Lany, and A. Zunger, Phys. Rev. B **72**, 035211 (2005).
[20] W. Kohn and L. J. Sham, Phys. Rev. **140**, A1133 (1965).
[21] The ABINIT code is a common project of the Université Catholique de Louvain, Corning Incorporated, and other contributors (http://www.abinit.org). See, also, X. Gonze *et al.*, Comput. Mater. Sci. **25**, 478 (2002).
[22] J. P. Perdew, K. Burke, and M. Ernzerhof, Phys. Rev. Lett. **77**, 3865 (1996).
[23] N. Troullier and J. L. Martins, Phys. Rev. B **43**, 1993 (1991); **43**, 8861 (1991).
[24] T. Maekawa, K. Kurosaki, and S. Yamanaka, J. Alloys Compd. **416**, 214 (2006).
[25] G. Makov and M. C. Payne, Phys. Rev. B **51**, 4014 (1995).
[26] J. X. Zheng, G. Ceder, T. Maxisch, W. K. Chim, and W. K. Choi, Phys. Rev. B **75**, 104112 (2007).
[27] P. G. Sundell, M. E. Björketun, and G. Wahnström, Phys. Rev. B **73**, 104112 (2006).
[28] T. Norby, M. Wideroe, R. Glöckner, and Y. Larring, Dalton Trans. **19**, 3012 (2004).
[29] K. D. Kreuer, Annu. Rev. Mater. Res. **33**, 333 (2003).
[30] J. F. Janak, Phys. Rev. B **18**, 7165 (1978).
[31] A. Zywietz, J. Furthmüller, and F. Bechstedt, Phys. Rev. B **59**, 15166 (1999).
[32] R. D. Shannon, Acta Crystallogr., Sect. A: Cryst. Phys., Diffr., Theor. Gen. Crystallogr. **32**, 751 (1976).
[33] M. A. Gomez, M. A. Griffin, S. Jindal, K. D. Rule, and V. R. Cooper, J. Chem. Phys. **123**, 094703 (2005).
[34] C. Shi, M. Yoshino, and M. Morinaga, Solid State Ionics **176**, 1091 (2005).
[35] R. Hempelmann, Physica B (Amsterdam) **226**, 72 (1996).
[36] A. Longo, F. Giannici, A. Balerna, C. Ingrao, F. Deganello, and A. Martorana, Chem. Mater. **18**, 5782 (2006).
[37] F. Giannici, A. Longo, F. Deganello, A. Balerna, A. S. Arico, and A. Martorana, Solid State Ionics **178**, 587 (2007).
[38] R. Glöckner, M. S. Islam, and T. Norby, Solid State Ionics **122**, 145 (1999).
[39] R. A. Davies, M. S. Islam, and J. D. Gale, Solid State Ionics **126**, 323 (1999).